dortmund university

Course Summary from Winter Semester 2023/2024

Key Experiments in Particle Physics

Joel Koch

29.02.2024

Experimental Physics IV
Faculty Physics
University Dortmund

Contents

1 The Wu Experiment

The Wu experiment focuses on the parity transformation $\hat{P}$, charge conjugation transformation $\hat{C}$ and its combination $\hat{C}\hat{P}$. In physics, parity describes the symmetry of spatial coordinates. A given point $(t, \vec{x})$ would transform to $(t, -\vec{x})$ under $\hat{P}$. Classical physics is invariant under parity transformation and is thus conserving it. The intrinsic parity of a particle is calculated via the spin l by $\hat{P} = (-1)^l$. As classical physics is invariant under the change of sign in spatial coordinates, it is also invariant under the change of sign of electric charges. In elementary particle physics, the change of sign of electric charges is called charge conjugation transformation $\hat{C}$ converting particles into anti-particles and vice versa, $\hat{C}\,|e\rangle = |\bar{e}\rangle$. By 1957, significant discoveries of particles had already taken place, such as $e^{\pm}$, ν_e, μ, p, γ, π and K. Parity conservation was evident for the electromagnetic (EM), the strong and the gravitational interaction, but there was no experimental evidence for parity conservation in the weak interaction [1]. For most physicists, it seemed self-evident that parity is conserved in the weak interaction as well. In 1956 however, Tsung-Dao Lee (*1926) and Chen Ning Yang (*1922) considered the possibility that $\hat{P}$ can be violated in the weak interaction and proposed different experiments to test it [2]. The first to carry out such an experiment was Chien-Shiung Wu (1912-1997) when she was approached by Lee and Yang for her expertise in β-decay in 1956. The experiment was based on the decay of Cobalt via $\mathrm{Co}^{60}_{27} \rightarrow \mathrm{Ni}^{60}_{28} + e^- + 2\gamma + \bar{\nu}_e$. Cobalt has a spin of 5 and was used because it decays via a β-decay into excited nickel with a spin of 4 meaning that the particles have to have the same spin direction. Due to the polarization of the nucleus, the electrons are emitted either upwards or downwards. The emission of the electrons is invariant under parity transformation if it is conserved in the weak interaction and vice versa. A cerium magnesium nitrate (CMN)-crystal with a small layer of cobalt was used as the specimen and placed inside a housing necessary to hold the polarization [1] which was

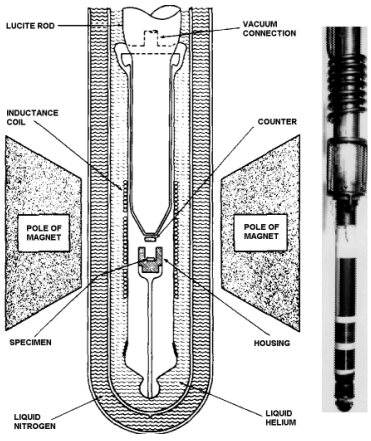

Figure 1.1: Schematic illustration and photograph of the apparatus [3].

caused by a magnetic field. A schematic illustration with a photograph of the used apparatus is shown in figure 1.1. An anthracene crystal was used as a scintillation counter and placed inside the lucite rod. Sodium iodide gamma-scintillation counters were installed externally to measure the γ. If the magnetic field is repolarized, the electron emission rates will stay the same if parity is conserved. The γ-scintillation counters were used to measure the state of the polarization because the originally isotropic emission changes under parity transformation to an oval anisotropy as this is an EM process that conserves parity [1]. The experimental results are shown in figure 1.2. The measured electron rates show a clear dependence on the polarization direction. This asymmetry in the emission of electrons is violating parity conservation as the electrons prefer a direction in which to be emitted [4]. By comparing the γ and β emissions for similarities, it can be seen that the β asymmetry reduces when the γ anisotropy reduces indicating that it is not due to misalignment of the apparatus. Further systematic checks have been made showing no dependence on systematic uncertainties [1]. Parity nonconservation in the weak interaction also implies the violation of charge conjugation assuming its combination is conserved.

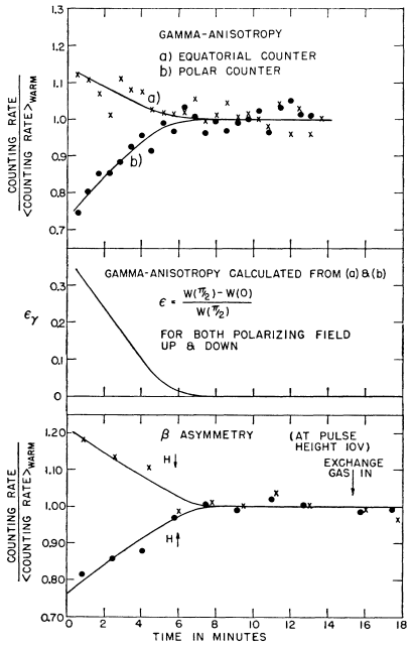

Figure 1.2: Measured results showing the gamma anisotropy and electron asymmetry for a polarizing magnetic field pointing up and down [4].

The measured asymmetry was quantified by comparing the β asymmetry with the γ anisotropy. But only a lower limit of $\alpha \leq -0.7$ could be measured because the anisotropy was difficult to measure. Lee and Yang received a Nobel Prize while Wu did not. A two-component neutrino theory published by Lee and Yang in 1957 introduces right-handed neutrinos and left-handed antineutrinos, both being massless and having a parity asymmetry of $\alpha = -1$ [5]. Thus, a new experiment was designed to measure an asymmetry value of $\alpha = -1{,}01 \pm 0{,}02$ [6] which is in perfect agreement with the theory leading to the (V-A)-structure introduced by Richard Feynman and Murray Gell-Mann. According to the Sakharov conditions from 1967¥ [7] the matter-antimatter asymmetry in the universe could be explained if, amongst other things, $\hat{C}$ and $\hat{C}\hat{P}$ can be violated which the Wu experiment demonstrated. The search for $\hat{C}\hat{P}$-asymmetry is still researched today as the largest asymmetry yet was measured at LHCb in 2022 [8].

2 The Discovery of the Gluon

To organize hadrons in dependence on the quantum variables strangeness and isospin Murray Gell-Mann and Yuval Ne'eman proposed independently from each other the Eightfold Way in 1961. Mesons with a spin parity configuration of 0^- and baryons with $^1/_2{}^+$ can both be organized in an octet while baryons with $^3/_2{}^+$ can be organized in a decuplet of which the tenth particle, the $\Omega^-(sss)$ has been proposed theoretically before it has been found later [9]. The early quark model was proposed by Gell-Mann and George Zweig in 1964 which consisted of only $u-$, $d-$, s-quark. An electron-proton scattering event from 1968 revealed partons that took up half of the carried momentum and were thus the first indication of gluons [10]. A theoretical description is given by Quantum Chromodynamics (QCD) after which the baryon wave function must be antisymmetric thus leading to the introduction of colour as another quantum variable that can be either red, green or blue. QCD is an SU(3) gauge symmetry theory that describes the strong interaction predicting eight gluons as gauge bosons that can interact with themselves. Particles with a colour charge can never be detected as a single particle, because the energy to separate two particles increases until a particle-antiparticle pair is produced, called confinement leading to quarks and gluons combining with other colour-carrying particles forming new hadrons. These hadrons can in turn form new hadrons themselves building a cascade of particles called a jet which was first observed at the Stanford Positron Electron Asymmetric Rings (SPEAR) at 7,4 GeV in 1975. In the year 1979, all quarks except the top quark were found in experiments with the most recent discovery being the bottom quark in 1977 with no experimental evidence for gluons thus far. Due to corrections at high energies, an electron-positron collision can produce a quark-antiquark pair with an additional gluon in a three-jet event as suggested by John Ellis. The gluon emission can be seen as the equivalent of bremsstrahlung in QCD. The transition between a two and a three-jet event is continuous as the jets get broader es the energy increases until they can split up into three distinct jets with one for each particle. A two jet-event starts at energies of 7,4 GeV and

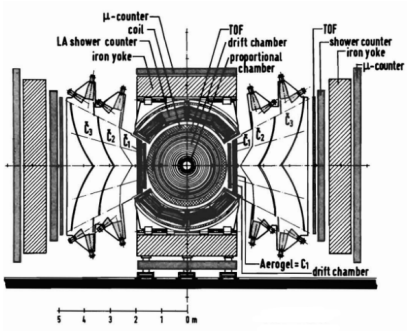

Figure 2.1: Schematic image of the TASSO-detector [11].

turns into a three-jet event at $\sim 20\,\text{GeV}$. The first gluon was discovered in a three-jet event at a center of mass energy of 27,4 GeV with the Two Arm Spectrometer Solenoid detector (TASSO) at the Positron-Electron Tandem Ring Accelerator (PETRA) in 1979 which is part of the Deutsches Elektronen-Synchrotron (DESY). A schematic picture of TASSO is shown in figure 2.1. It started building in 1976 and was finished just two years later and had a ring accelerator with a circumference of 2,304 km. The detector had two hadron-identifying arms, one aerogel and two gas Cherenkov detectors and time-of-flight and shower counters. Event shape variables were introduced as perturbation theory was not useable for low energies which could be used to distinguish between different QCD models, one in which there are no gluons and one in which there are. The experimental results were in good agreement with the gluon model, as can be seen in figure 2.2a that shows predictions for different models [12]. By measuring the angle in a Lorentz-boosted center-of-momentum frame, called the Ellis-Karliner angle, it is possible to analyse the spin of the gluon. The Ellis-Karliner angle distribution from TASSO is shown in figure 2.2b in which the experimental data matches the theoretical prediction of a vector particle proving that the gluon has a spin of 1 [10, 13]. The discovery of the gluon is the perfect example of theory and experiments working together to discover new parts of physics as the gluon was originally predicted by QCD as a vector boson that could be emitted in three-jet events and was discovered in such an event with the exact characteristics it was predicted to have.

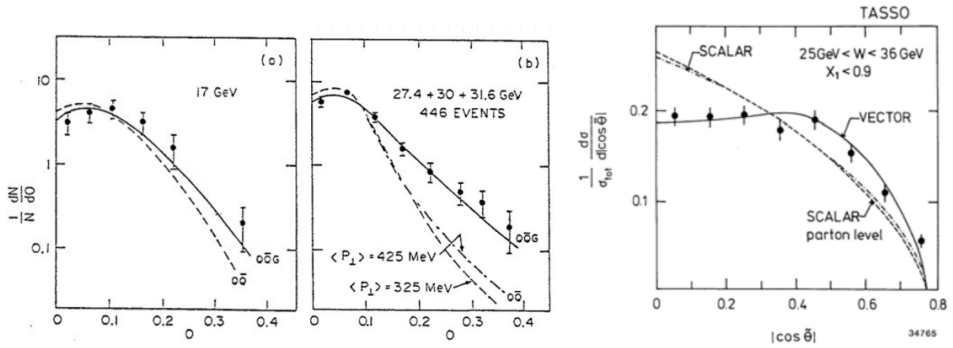

(a) Experimental results comparing comparing different QCD models[12].

(b) Ellis-Karliner angle distribution from TASSO [13].

Figure 2.2: Experimental results from the TASSO detector [12, 13].

The strong coupling constant α_S which determines the strength of the interaction can be calculated by measuring the cross-section of three- versus two-jet events. The compact muon solenoid experiment (CMS) at the large hadron collider (LHC) measured a value of $\alpha_S = 0{,}1448 \pm 0{,}0014$ at $\sqrt{s} = 7\,\text{TeV}$ in 2011 [14].

3 Semiconductor Detectors

The earliest studies of semiconductor detectors date back to 1833 when Faraday discovered the temperature dependence of the conductivity of silver sulphide. Nearly a hundred years later, Wilson described a band theory of solids in 1931, in which quantum mechanics explains the characteristics of semiconductors. The electrical conductivity can be described by the valence band (VB) which consists of positively charged quasiparticles that are called holes h^+ and the conduction band (CB) which is filled with electrons [15]. The band theory of solids distinguishes three types of conductive solids. Insulators with a band gap of $E_G \approx 9\,\text{eV}$, semiconductors with $E_G \approx 1\,\text{eV}$ and conductors with no gap. The properties of semiconductors can be changed by inserting impurities into the crystal structure. If an atom with five electrons, called a donor, is inserted into an element with four electrons, an excessive conduction electron appears. If an atom with three electrons, called an acceptor, is inserted into an element with three electrons, an excessive hole appears. Semiconductors doped with donors are called n-doped while those doped with acceptors are called p-doped. When both types of doped semiconductors are combined they form a diode. Drifting and combining of e^-/h^+ forms an electrical field at the junction of the semiconductor which is called the depletion zone. If an external positive voltage at the p side relative to the n side is applied, this electrical field is weakened and current can flow which is called forward bias. In reverse bias, the electrical field is strengthened and the depletion zone increases. This configuration is used in detectors to measure ionizing particles.

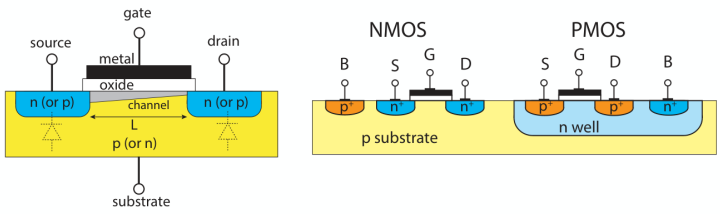

(a) MOSFET. (b) CMOS.

Figure 3.1: Schematic illustration of a MOSFET and a CMOS semiconductor [15].

The most used semiconductor detectors are complementary metal-oxide-semiconductors

(CMOS) consisting of a part with a p-doped substrate and an n-doped drain terminal (NMOS) and a part with the reverse (PMOS). Figure 3.1 shows a CMOS and a widely in field-effect transistor used semiconductor (MOSFET).

The simplest design of detectors is a pn area diode consisting of a 300 µm thick p and n-doped area. An additional guard ring can reduce the electrical noise. Dividing the area into strips or pixels (length < 100 µm) yields one or even two spatial coordinates but increases the readout difficulty. There are two different types to read out the information from the collection diodes. Hybrid pixel sensors have the readout electronics on a different chip which is a laborious assembly and resides in a large material thickness, the sensor, however, can be separately optimized to the readout components. Monolithic pixel sensors reduce their material by an entire order of magnitude but not all production lines are suited to produce such sensors. As pixel detectors are used to reconstruct traces for example in the ATLAS Experiment due to their good resolution with an uncertainty of $\sigma_x = {}^{\text{pitch}}/\sqrt{12}$ [16], they are placed closest to the collision vertex where a lot of charged particles pass through them causing damage to the detector substrate. Such radiation damage can cause a change in effective doping concentration leading to deactivated donor or acceptor atoms. They can furthermore cause trapping where e^-/h^+ are trapped in defects of the crystal structure and are released later. These defects can form energy levels that excite e^-/h^+ easier and cause a flow in current. Radiation damage can be reduced by cooling [16].

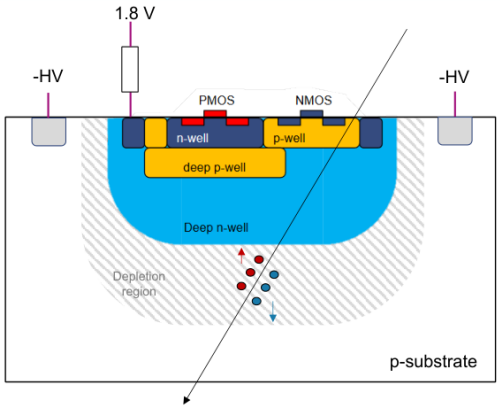

Figure 3.2: Schematic illustration of a MightyPix [17].

A track is reconstructed by forming groups of measurement points, called tracklets which require a good spatial and time resolution of the pixel detectors. In each of the tracklets every possible combination is built but only those that point to the interacting point are accepted, forming a track when a series of tracklets match. An application of pixel detectors is given in the example of MightyPix, a design sketch of possible pixel detectors used in the second upgrade of the LHC that is shown in figure 3.2. Their requirements for the upgrade include a time resolution of < 3 ns, and a pixel size of $50\,\text{µm} \times 150\,\text{µm}$. Semiconductor detectors in the form of pixel detectors provide good time and space resolution which is why particle detectors are indispensable without them. However, the implementation of pixel detectors brings new challenges like the power distribution or the cooling.

4 Oscillation of neutral B-mesons

The phenomenon of neutral mesons transforming into their respective antiparticle was first investigated by Gell-Main and Pais in 1955 [18]. The CKM-matrix was introduced as an extension of the Cabbibo matrix in 1973 after discovering CP violation which could not be explained with 4-quark-mixing [19]. Each element of the matrix describes a transition between quark generations. The neutral B meson $B_d^0(d\bar{b})$ or respectively $B_s^0(s\bar{d})$ can oscillate via two components, the on-shell ($E^2 = p^2 + m^2$) and off-shell ($E^2 \neq p^2 + m^2$) components. Both are shown in 4.1a and 4.1b respectively. Measuring the oscillation frequency yields precise

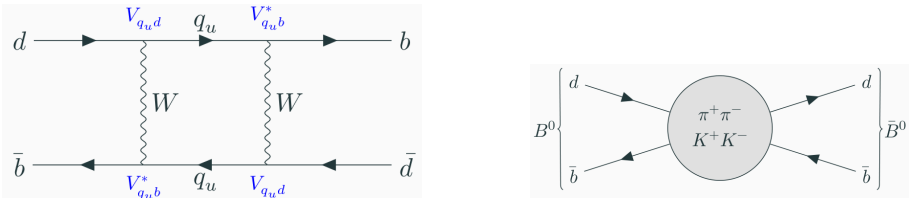

(a) On-shell contribution. **(b)** Off-shell contribution.

Figure 4.1: Feynman diagram showing the neutral B meson oscillation [20].

measurements of $V_{q_u b}$ and $V_{q_u d/s}$. A time evolution can be deduced by introducing a mixing matrix in which non-diagonal elements occur due to oscillations via the box diagram 4.1a and the on-shell contributions. By diagonalising the mixing matrix an expression for the time evolution of flavour eigenstates can be found. An expression for the oscillation frequency can be found due to the on-shell contribution being much smaller than the off-shell contributions ($\Gamma_{ij} < M_{ij}$) of $\Delta m_{d/s} \propto |V_{td}|^2$ with $\Delta m_{d/s}$ describing a mass difference [21]. The B_d^0 oscillation was first discovered at the ARGUS detector at DESY in 1987 [22]. Earlier measurements were done by CLEO [23], MARK II [24] and UA1 [25] collaborations. Collisions of e^+e^- at an energy of the $\Upsilon(4S)$ resonance produced $B_d^0 B_d^0$ pairs which were used to measure the oscillation. One of the methods to look for B_d^0 oscillation was to search for a fully reconstructed decay of $\Upsilon(4S) \to B_d^0 B_d^0 / \bar{B}_d^0 \bar{B}_d^0$ which decayed flavourspecific via $B_d^0 \to D^{*-}\pi^+ / D^{*-} l^+ \nu$ and $\bar{B}_d^0 \to D^{*+}\pi^- / D^{*+} l^- \nu$. A different method was to reconstruct one B_d^0 from the $\Upsilon(4S)$ and tag the other B_d^0 with a lepton. Using the same decay channels for the reconstruction of B_d^0 makes this method less sensitive to background originating from lepton misidentification. It yielded a time-integrated

oscillation parameter $r = \frac{\mathcal{BR}(B \to \bar{B} \to \bar{X})}{\mathcal{BR}(B \to X)}$ of $r = 0{,}21 \pm 0{,}08$ which meant for the matrix element $V_{td} \neq 0$ [22].

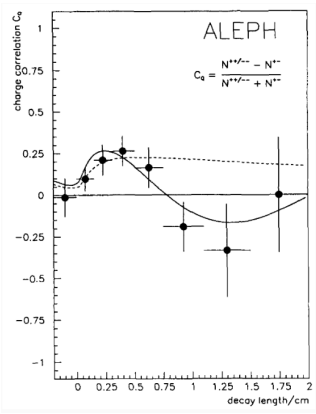

Figure 4.2: Fit to $Q_C(t)$ with a time dependent oscillation in data (solid) and a time independent approach (dashed) [26].

The ALEPH experiment at LEP measured the oscillation frequency Δm_d by tagging the state of B_d^0 at the time of production which decays semileptonic and at the time of decay which decays flavourspecific via $B_d^0 \to D^{*-}X$ and $\bar{B}_d^0 \to D^{*+}X$ [26]. Every *correct* sign in the decay was defined as an unmixed event and vice versa by which a charge correlation function $C_Q(t)$ was defined. At ALEPH the B_d^0 momentum was not reconstructed and the decay time was not calculated and only the decay length was used with boosting of B_d^0 that involved the momentum spectra. Figure 4.2 shows an unbinned maximum likelihood fit to the decay length distribution to get $C_Q(t)$. The involvement of the decay length distribution with the momentum spectra yielded the decay time. An oscillation frequency of $\Delta m_d = 0.52^{+0.10}_{-0.11}(\text{stat})^{+0.04}_{-0.05}(\text{syst})\,\text{ps}^{-1}$ was found [26].

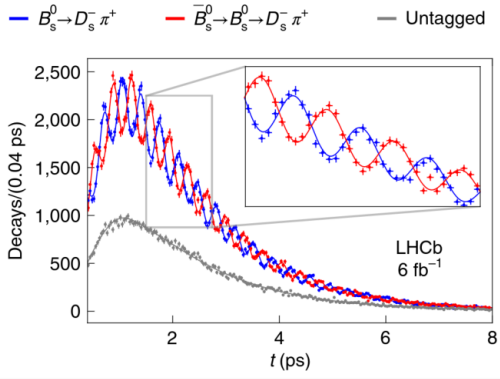

Figure 4.3: Measurement of B_s^0 oscillations with the LHCb experiment [27].

The oscillation of B_s^0 is more likely than the B_d^0 oscillation, due to $|V_{ts}| > |V_{td}|$ and was first discovered at CDF II in 2006 [28]. Due to the mass difference of s quarks being larger than those of d quarks, a better time resolution was needed. Measurements of Δm_d with the LHCb experiment at the LHC could increase the precision in 2016 [29] to a value of $\Delta m_d = 0.505 \pm 0.0021\,(\text{stat}) \pm 0.001\,(\text{syst})\,\text{ps}^{-1}$ leading to a matrix element of $V_{td} = (8{,}6 \pm 0{,}2) \cdot 10^{-3}$ [30]. A study from 2022 found an oscillation frequency for B_s^0 of $\Delta m_s = 17.7683 \pm 0.0051\,(\text{stat}) \pm 0.0032\,(\text{syst})\,\text{ps}^{-1}$ [27] which lead to a value for the matrix element of $V_{ts} = (41{,}5 \pm 0{,}9) \cdot 10^{-3}$ [30]. In figure 4.3 the measurements of B_s^0 oscillations from the LHCb experiment are shown. Figure 4.3 shows the decay time of the $B_s^0 \to D_s^- \pi^+$ signal decays are shown with the unmixed components shown in blue and the mixed components shown in red.

Bibliography

[1] Ronald Laymon and Franklin Allan. *Case Studies in Experimental Physics. Why Scientists Pursue Investigation*. 1st. Springer Cham, 2022. DOI: https://doi.org/10.1007/978-3-031-12608-6.

[2] T. D. Lee and C. N. Yang. 'Question of Parity Conservation in Weak Interactions'. In: *Phys. Rev.* 104 (1 1956), pp. 254–258. DOI: 10.1103/PhysRev.104.254. URL: https://link.aps.org/doi/10.1103/PhysRev.104.254.

[3] 'The Reversal of Parity Law in Nuclear Physics'. In: (2023). URL: https://www.nist.gov/pml/fall-parity/reversal-parity-law-nuclear-physics.

[4] C. S. Wu et al. 'Experimental Test of Parity Conservation in Beta Decay'. In: *Phys. Rev.* 105 (4 1957), pp. 1413–1415. DOI: 10.1103/PhysRev.105.1413. URL: https://link.aps.org/doi/10.1103/PhysRev.105.1413.

[5] T. D. Lee and C. N. Yang. 'Parity Nonconservation and a Two-Component Theory of the Neutrino'. In: *Phys. Rev.* 105 (5 1957), pp. 1671–1675. DOI: 10.1103/PhysRev.105.1671. URL: https://link.aps.org/doi/10.1103/PhysRev.105.1671.

[6] L.M. Chirovsky et al. 'Directional distributions of beta-rays emitted from polarized 60Co nuclei'. In: *Physics Letters B* 94.2 (1980), pp. 127–130. ISSN: 0370-2693. DOI: https://doi.org/10.1016/0370-2693(80)90840-0. URL: https://www.sciencedirect.com/science/article/pii/0370269380908400.

[7] Beatriz Gato-Rivera. *Antimatter. What It Is and Why It's Important in Physics and Everyday Life*. 1st ed. 2021. DOI: https://doi.org/10.1007/978-3-030-67791-6.

[8] Piotr Tracyzk. 'Largest matti-antimatter asymmetry observed'. In: (2022). URL: https://home.cern/news/news/physics/largest-matter-antimatter-asymmetry-observed.

[9] Harald Fritzsch. 'Introduction to Quark Model'. In: *Murray Gell-Mann and the Physics of Quarks*. Cham: Springer International Publishing, 2018, pp. 43–48. ISBN: 978-3-319-92195-2. DOI: 10.1007/978-3-319-92195-2_4. URL: https://doi.org/10.1007/978-3-319-92195-2_4.

[10] David Venker. 'The discovery of the gluon. Lecture on the seminar key experiments in particle physics'. 2023.

[11] G. Wolf et al. 'TASSO RESULTS ON e+ e- ANNIHILATION BETWEEN 13-GeV AND 31.6-GeV AND EVIDENCE FOR THREE JET EVENTS'. In: *eConf* C790823 (1979). Ed. by T. B. W. Kirk and H. D. I. Abarbanel, p. 34.

[12] James G. Branson. 'Gluon Jets'. In: *NATO Sci. Ser. B* 352 (1996). Ed. by Harvey B. Newman and Thomas Ypsilantis, pp. 101–121. DOI: 10.1007/978-1-4613-1147-8_8.

[13] P. Soding et al. 'The First evidence for three jet events in e+ e- collisions at PETRA: First direct observation of the gluon'. In: *International Europhysics Conference on High-energy Physics (HEP 95)*. Sept. 1996, pp. 3–14.

[14] Serguei Chatrchyan et al. 'Measurement of the Ratio of the Inclusive 3-Jet Cross Section to the Inclusive 2-Jet Cross Section in pp Collisions at $\sqrt{s} =$ 7 TeV and First Determination of the Strong Coupling Constant in the TeV Range'. In: *Eur. Phys. J. C* 73.10 (2013), p. 2604. DOI: 10.1140/epjc/s10052-013-2604-6. arXiv: 1304.7498 [hep-ex].

[15] Hermann Kolanoski and Norbert Wermes. *Particle Detectors: Fundamentals and Applications*. Oxford University Press, June 2020. ISBN: 9780198858362. DOI: 10.1093/oso/9780198858362.001.0001.

[16] Tom Troska. 'Semiconductor detectors. Seminarvortrag: Schlüsselexperimente in der Teilchenphysik'. Dec. 2023.

[17] Richard Leys et al. *MightyPix: A HV-CMOS Pixel Chip for LHCb's Mighty Tracker*. 2023. URL: https://indico.cern.ch/event/1223972/contributions/5262041/attachments/2602200/4493474/MightyPix_SigridScherl.pdf.

[18] M. Gell-Mann and A. Pais. 'Behavior of Neutral Particles under Charge Conjugation'. In: *Phys. Rev.* 97 (5 Mar. 1955), pp. 1387–1389. DOI: 10.1103/PhysRev.97.1387. URL: https://link.aps.org/doi/10.1103/PhysRev.97.1387.

[19] Makoto Kobayashi and Toshihide Maskawa. 'CP-Violation in the Renormalizable Theory of Weak Interaction'. In: *Progress of Theoretical Physics* 49.2 (Feb. 1973), pp. 652–657. ISSN: 0033-068X. DOI: 10.1143/PTP.49.652. eprint: https://academic.oup.com/ptp/article-pdf/49/2/652/5257692/49-2-652.pdf. URL: https://doi.org/10.1143/PTP.49.652.

[20] Katharina Popp. 'Oscillation of neutral B mesons'. Dec. 2023.

[21] Marina Artuso, Guennadi Borissov and Alexander Lenz. *CP Violation in the B_s^0 system*. 2019. arXiv: 1511.09466 [hep-ph].

[22] H. Albrecht et al. 'Observation of B0-B0 mixing'. In: *Physics Letters B* 192.1 (1987), pp. 245–252. ISSN: 0370-2693. DOI: https://doi.org/10.1016/0370-2693(87)91177-4. URL: https://www.sciencedirect.com/science/article/pii/0370269387911774.

[23] A. Bean et al. 'Limits on $B^0\mathrm{B}^0$ mixing and &'. In: *Phys. Rev. Lett.* 58 (3 Jan. 1987), pp. 183–186. DOI: 10.1103/PhysRevLett.58.183. URL: https://link.aps.org/doi/10.1103/PhysRevLett.58.183.

[24] T. Schaad et al. 'Upper limit on B0B0 mixing in e+e− annihilation at 29 GeV'. In: *Physics Letters B* 160.1 (1985), pp. 188–192. ISSN: 0370-2693. DOI: https://doi.org/10.1016/0370-2693(85)91490-X. URL: https://www.sciencedirect.com/science/article/pii/037026938591490X.

[25] C. Albajar et al. 'Search for B0—B¯0 oscillations at the CERN proton-antiproton collider'. In: *Physics Letters B* 186.2 (1987), pp. 247–254. ISSN: 0370-2693. DOI: https://doi.org/10.1016/0370-2693(87)90288-7. URL: https://www.sciencedirect.com/science/article/pii/0370269387902887.

[26] D. Buskulic et al. 'Observation of the time dependence of B0d—B0d mixing'. In: *Physics Letters B* 313.3 (1993), pp. 498–508. ISSN: 0370-2693. DOI: https://doi.org/10.1016/0370-2693(93)90025-D. URL: https://www.sciencedirect.com/science/article/pii/037026939390025D.

[27] R et al. Aaij. 'Precise determination of the B_s^0–$\overline{B}_s^0$ oscillation frequency'. In: *Nature Physics* 18 (2022), pp. 1–5. DOI: https://doi.org/10.1038/s41567-021-01394-x.

[28] A. Abulencia et al. 'Observation of $B_s^0 - \overline{B}_s^0$ Oscillations'. In: *Phys. Rev. Lett.* 97 (24 Dec. 2006), p. 242003. DOI: 10.1103/PhysRevLett.97.242003. URL: https://link.aps.org/doi/10.1103/PhysRevLett.97.242003.

[29] R et al. Aaij. 'A precise measurement of the B_s^0 meson oscillation frequency'. In: *The European Physical Journal C* 76 (2016). DOI: https://doi.org/10.1140/epjc/s10052-016-4250-2.

[30] R. L. Workman et al. 'Review of Particle Physics'. In: *PTEP* 2022 (2022), p. 083C01. DOI: 10.1093/ptep/ptac097.